Osteoarthritis and Cartilage (2008) **16,** 506–514

doi:10.1016/j.joca.2007.08.005

Osteoarthritis and Cartilage

International Cartilage Repair Society

OARSI OSTEOARTHRITIS RESEARCH SOCIETY INTERNATIONAL

Cartilage damage pattern in relation to subchondral plate thickness in a collagenase-induced model of osteoarthritis

S. M. Botter M.Sc.†‡, G. J. V. M. van Osch Ph.D.†‖, J. H. Waarsing Ph.D.†, J. C. van der Linden Ph.D.†§, J. A. N. Verhaar M.D.†, H. A. P. Pols M.D.‡, J. P. T. M. van Leeuwen Ph.D.‡ and H. Weinans Ph.D.†*

† *Erasmus MC, University Medical Centre Rotterdam, Department of Orthopaedics, The Netherlands*

‡ *Erasmus MC, University Medical Centre Rotterdam, Department of Internal Medicine, The Netherlands*

§ *Delft University of Technology, Faculty 3ME, Department Precision and Microsystems Engineering, The Netherlands*

‖ *Erasmus MC, University Medical Centre Rotterdam, Department of Otorhinolaryngology, The Netherlands*

Summary

Objective: To see how initial differences in subchondral bone phenotype influence the development of cartilage damage and changes in subchondral bone architecture in an osteoarthritis (OA)-induced mouse model.

Method: Intra-articular collagenase injections (right knee joint) and saline controls (left knee joint) were applied in the knees of two mouse strains known to have either a low or a high bone mass phenotype: the low bone mass C57Bl/6 mice with a thin subchondral bone plate and high bone mass C3H/HeJ mice with a thick subchondral bone plate. The ages of the mice were 16 and 30 weeks, with $n = 8$ per group. The collagenase injection induced an osteoarthritic phenotype that was evaluated 4 weeks later in the tibia using histological analyses and micro-computed tomography (micro-CT).

Results: Both strains developed cartilage damage in the collagenase-injected right knee joints to a comparable extent, however, the spatial distribution of cartilage damage differed significantly: C57Bl/6 mice had most damage at the postero-lateral side, whereas in C3H/HeJ mice the postero-medial region was the most affected. Spontaneous cartilage damage was found in the saline-injected left control knees of C57Bl/6 mice, but in C3H/HeJ mice spontaneous cartilage damage was virtually absent. In both strains the subchondral bone plate of collagenase-injected joints became thinner, independent of the site of cartilage damage. TRAP-positive osteoclasts were observed underneath the subchondral bone plate, in line with the observed decreased thickness. No link was found between subchondral bone plate thickness and cartilage damage in the collagenase-injected joints. The subchondral trabecular architecture only changed in the high bone mass C3H/HeJ mice, with thinning of trabeculae and increased trabecular spacing.

Conclusion: Thinning of the subchondral bone plate was found as a common observation 4 weeks after OA had been induced in two strains of mice having either a high or low bone phenotype, but no relation was found with the amount of cartilage damage. In addition, this study shows that different strains of mice can react differently to instability-induced OA with respect to the spatial arrangement of cartilage damage and changes in subchondral trabecular structure.

Key words: Bone, Subchondral bone, Micro-computed tomography, Animal studies, Osteoarthritis.

Introduction

Osteoarthritis (OA) is one among the leading causes of disability in the elderly and forms a major burden to health care. About 30% of persons aged 65 and over are affected with knee or hip OA[1]. A disease modifying treatment is not yet available and treatment is focussed on reduction of symptoms. Therefore, more basal knowledge about its possible cause(s) is needed.

Located directly underneath the cartilage, the subchondral bone plate was initially thought to play a role in OA initiation and progression[2]. The proposed idea was that stiffness variations in the subchondral bone plate would lead to the initiation of cartilage fibrillation. During the disease process the bone plate would then become stiffer, causing a reduced shock-absorbing capacity and leading to progression of these lesions. However, more recent work shows that the stiffness of subchondral bone in OA is actually decreased, because of an increased porosity and a reduced mineral content[3–7].

Apart from changes in composition, the amount of subchondral bone also changes and subchondral sclerosis is universally recognized as being a typical OA characteristic. This is also seen in animals, for instance in macaques who develop OA spontaneously[8]. Specifically, thickening of the subchondral bone plate has been observed in guinea pigs[9,10], rabbits[11], and mice[12]. Besides having more bone at the location of disease, OA patients also seem to have a higher bone mass at other sites of the skeleton[13–16].

*Address correspondence and reprint requests to: H. Weinans, Ph.D., Erasmus MC, University Medical Center Rotterdam, Erasmus Orthopaedic Research Lab, EE-1614, P.O. Box 2040, 3000 CA Rotterdam, The Netherlands. Tel: 31-0-10-40-87367/87384; Fax: 31-0-10-40-89415; E-mail: h.weinans@erasmusmc.nl

Received 10 January 2007; revision accepted 4 August 2007.

A study by Bergink *et al.* even suggests that a high systemic bone mineral density (BMD) before disease initiation is associated with increased incidence and progression of knee OA[17].

From these studies it is clear that changes in the subchondral bone play a role in OA, and that bone phenotype may influence disease onset and/or progression. However, the relation between subchondral bone architecture, subchondral bone plate thickness and the resulting pattern of cartilage damage during OA development is not clear. The aim of the current study was therefore to study these issues in a murine model of collagenase-induced OA[18,19]. Specifically, to investigate the relation between subchondral bone phenotype and development of OA, we compared two mouse strains: the C57Bl/6 strain that has a low bone mass and a thin subchondral bone plate and the C3H/HeJ strain that has a high bone mass as well as a thicker bone plate, at two different ages.

Methods

ANIMALS

Following the approval of the local animal ethics committee, male C3H/HeJCrlBR mice (Charles River, Sulzfeld, Germany) and C57Bl/6 mice (Harlan, Zeist, The Netherlands) aged 16 and 30 weeks were used with eight mice per group. The animals were maintained on a 12:12 h light:dark cycle, housed in individually ventilated cages with three brother littermates per cage and were fed *ad libitum*.

For induction of OA, we used the collagenase OA model as described previously[18,19]. This model utilizes bacterial collagenase injected into the knee joint space, thereby inducing damage to joint structures containing type I collagen such as tendons, ligaments and menisci, and causes an increase in knee joint laxity resulting in cartilage damage[20,21]. The enzyme has minimal direct effect on articular cartilage, which contains type II collagen that is resistant to digestion by the bacterial enzyme[22]. Test-injections in cadavric mice using the dye toluidine blue confirmed the injected fluid to be present in the knee joint space only. At 16 or 30 weeks of age, the animals were anesthetized with a 5% isoflurane/N_2O/O_2 mixture. A small incision was made in the skin at the anterior side of the knee joint such that the patellar tendon was exposed and an accurate injection could be applied. Six microlitres containing 10 U of highly purified bacterial type VII collagenase (Sigma, St Louis, MO) was injected into the right knee intra-articular space, the left knee was injected with 6 μl saline.

As an analgesic the animals received one subcutaneous injection of buprenorphine (Temgesic, 0.01 mg/kg body weight) directly after the collagenase injection. After 4 weeks the mice were euthanized and their knee joints were excised and fixed in 4% formalin for 2 days.

MICRO-COMPUTED TOMOGRAPHIC (MICRO-CT) SCANNING AND QUANTIFICATION OF BONE MORPHOMETRIC PARAMETERS

The knee joints were scanned with a voxel size of 9 μm using the Skyscan 1072 micro-CT scanner (Skyscan, Aartselaar, Belgium). In order to distinguish calcified tissue from noncalcified tissue, the reconstructed greyscale images were segmented by an automated algorithm using local thresholds[23]. The epiphysis of the tibia was chosen as the region of interest to study subchondral bone. The outline of the epiphysis was manually selected using 3D data analysis software (CTAnalyzer, Skyscan) and care was taken not to select outgrowing osteophytes (Fig. 1(a)).

Also, 1.0 mm of the proximal metaphyseal bone directly underneath the growth plate was selected, as well as 0.3 mm of diaphyseal cortical bone (Fig. 1(b)).

The subchondral bone plate and trabeculae of the epiphysis, and cortex and trabeculae of the metaphysis were separated using in-house developed automated software. Bone morphometric parameters of the thus obtained bone structures were determined using the freely available software package 3D-Calculator (http://www2.eur.nl/fgg/orthopaedics/). The following 3D morphometric parameters were calculated for the trabecular compartments: bone volume fraction (Trab BV/TV), which is the ratio of trabecular bone volume (Trab BV) over endocortical total volume (TV), trabecular thickness (Tb.Th.), trabecular spacing (Tb.Sp.), trabecular number (Tb.N.), connectivity density (CD), which calculates the number of trabecular connections per unit volume[24] and structure model index (SMI), indicating whether trabeculae have a rod-like or plate-like shape[25]. The thickness of the medial and lateral subchondral bone plate, as well as the diaphyseal cortex, was measured using the same algorithm as used for determining Tb.Th. A subset (0.5 mm medio-lateral width, 1.0 mm ventro-dorsal length) of the load-bearing region at the medial and lateral sides of the tibial plateau was taken as region of interest.

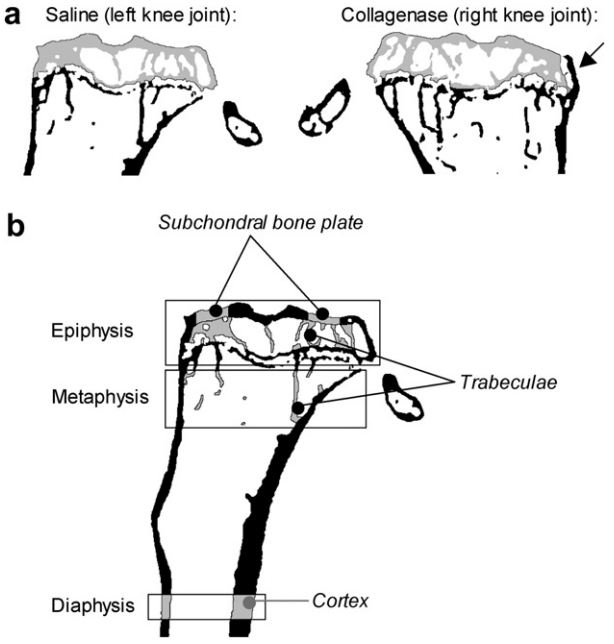

Fig. 1. Selection procedure of the epiphysis, metaphysis and diaphysis of the tibia for 3D morphometric analysis: (a) first, the epiphysis (left, grey) was manually selected as representative of subchondral bone, outgrowing osteophytes were excluded (right, arrow); (b) epiphyseal and metaphyseal trabeculae were separated from the subchondral bone plate and cortex, respectively. Each of the thus obtained bone regions was analyzed separately.

HISTOLOGICAL ANALYSIS

Following the scanning procedure, knee joints were embedded in methyl methacrylate and frontal sections were made to verify the presence of OA characteristics such as cartilage damage and osteophytes. Per knee joint 8–10 undecalcified sections of 6 μm thickness were obtained, with 100 μm interspacing. Of the obtained sections six were analyzed per joint, three in the anterior region and three in the posterior region in the load-bearing region of the joint. Goldner staining was performed which gave excellent discrimination between noncalcified cartilage, calcified cartilage and subchondral bone. Thicknesses of noncalcified and calcified cartilages were measured in one anterior and one posterior section using Bioquant Osteo v7.20 (Bioquant, Nashville, TN). This programme measures the thickness every 5 μm over a distance of 400 μm, producing roughly 80 measurements, which were then averaged.

Cartilage damage was quantified in the antero-medial, postero-medial, antero-lateral and postero-lateral regions of the tibial plateau using the semi-quantitative grading and staging system devised by the OARSI Working Group[26]. In this system the grade–score, reflecting the severity of the damage, ranges from 0 (no cartilage damage) to 4 (all cartilage lost, complete disorganization and deformation of the joint). A separately assigned stage score, reflecting the extent of damage, ranges from 0 (whole cartilage surface intact) to 4 (>50% of cartilage surface affected). Grade and stage scores are then multiplied, giving a maximum cartilage damage score of 24 for each of the four analyzed regions of the tibial plateau. We summed the damage scores of the four regions to reflect the total cartilage degeneration in the tibia, with a maximum obtainable summed damage score of 96.

Osteophyte presence was scored as follows: each of the six sections analyzed for cartilage damage was also analyzed for the presence of osteophytes at the medial and lateral sides of the tibia. In case an osteophyte was observed in any of these six sections, the knee joint was considered osteophyte-bearing. The percentage of osteophyte-positive knee joints was calculated for each group.

TRAP stainings were performed to visualize osteoclastic activity. Bone sections were deacrylated and stained using 1.1 mM Naphthol AS-BI phosphate (Sigma, St Louis, MO) as substrate, 5.2 mM pararosanilin as coupler,

and 46.5 mM sodium L-tartrate as an inhibitor according to Scheven *et al.*[27]. Nuclei were stained with methylene green.

DATA ANALYSIS

Differences between left and right knee joints within strains were analyzed with the Wilcoxon matched paired test. The Mann–Whitney *U* test was applied for differences between age groups, both within strains and between strains. In all cases, $P < 0.05$ was considered statistically significant. In all graphs, the error bars depict standard error of the mean (SEM).

Results

EFFECT OF THE OPERATION

Twelve hours after the operation, which corresponds to the therapeutic effective time span of the used analgesic, the animals were observed closely. Cage activity was normal apart from slight limping of the right leg and no further analgesia was applied. After a few days normal walking patterns returned. Although weight loss (2–6% of the original body weight) was measured in the first week after the operation, all animals had normal weight gain thereafter.

BASAL TIBIAL BONE MORPHOMETRY

All basal tibial bone morphometric parameters were derived from the control knee joints 4 weeks after the saline injection. As reported previously, C3H/HeJ mice had a thicker metaphyseal and diaphyseal cortex than C57Bl/6 mice confirming the high bone mass phenotype of the C3H/HeJ mice (Table I, metaphysis C3H/HeJ approx. 155 vs 130 μm C57Bl/6, diaphysis 260 vs 190 μm). In accordance, the subchondral bone plate of the epiphysis was significantly thicker in C3H/HeJ than in C57Bl/6 mice, both at the medial (C3H/HeJ: approx. 180 μm, C57Bl/6: 150 μm) and at the lateral side (C3H/HeJ: approx. 150 μm, C57Bl/6: 110 μm). In both mouse strains and at both ages the medial side of the subchondral bone plate was thicker than the lateral side. The morphometric parameters between the ages of 16 and 30 weeks confirmed aging effects in trabecular bone architecture in C57Bl/6 mice only. At 16 weeks of age the amount of trabecular bone (Trab BV/TV) in either epiphysis (30%) or metaphysis (15%) was not different between strains, but at 30 weeks C57Bl/6 mice had lost trabecular bone at both anatomical sites. This was paralleled by a decrease in trabecular connectivity and an increase in trabecular spacing, although Tb.Th. remained the same. In contrast, C3H/HeJ mice did not show a change in trabecular bone architecture between 16 and 30 weeks, neither in the epiphysis nor in the metaphysis. However, in this strain the lateral side of the subchondral bone plate became significantly thinner with age from 16 weeks (168 μm) to 30 weeks (149 μm) whereas the thickness at the medial side remained unchanged. C57Bl/6 mice did not show such a decrease in bone plate thickness. Finally, the thickness of both the metaphyseal and diaphyseal cortices did not change due to aging in either strain. Table I summarizes the examined bone morphometric parameters.

HISTOLOGICAL CHANGES

Quantification of total cartilage thickness (i.e., calcified plus noncalcified) on histology revealed no significant difference between the two strains at both ages, neither at the medial nor at the lateral side of the tibial plateau (data not shown). However, a difference in the ratio between calcified and noncalcified cartilage thicknesses was noted: C57Bl/6 mice had significantly thicker calcified cartilage, and significantly thinner noncalcified cartilage compared to C3H/HeJ mice, primarily at the medial side (Fig. 2). In collagenase-injected joints, no significant change was observed in the thickness of calcified cartilage compared to saline-injected

Table I

Basal tibial bone morphometry in male C57Bl/6 and C3H/HeJ mice. All parameters were derived from the saline-injected left knee joints, four weeks after injection. Values shown are averages ± SEM. Trab BV/TV = trabecular bone volume fraction, Tb.Th. = trabecular thickness, Tb.Sp. = trabecular spacing, CD = connectivity density, Ct.Th. = cortical thickness, Sb.Pl.Th. = subchondral plate thickness, med = medial, lat = lateral, #P < 0.05 age within strain, &P < 0.05 med vs lat within strain, ns = not significant

Location	Parameter	Age	C57Bl/6	C3H/HeJ	Strain difference
Epiphysis	Trab BV/TV (%)	16wks (+4)	30.3 ± 0.6	30.7 ± 1.1	ns
		30wks (+4)	27.1 ± 0.5#	30.5 ± 0.9	$P < 0.01$
	Tb.Th. (μm)	16wks (+4)	66.2 ± 0.6	72.1 ± 1.8	$P < 0.01$
		30wks (+4)	68.3 ± 0.6#	74.4 ± 1.2	$P < 0.01$
	Tb.Sp. (μm)	16wks (+4)	195.7 ± 3.6	205.9 ± 5.2	ns
		30wks (+4)	207.8 ± 3.1#	210.1 ± 5.2	ns
	CD	16wks (+4)	189.6 ± 16.3	99.8 ± 21.0	$P < 0.01$
		30wks (+4)	88.6 ± 6.8#	104.7 ± 18.2	ns
	Sb.Pl.Th., med (μm)	16wks (+4)	144.0 ± 5.3	188.8 ± 6.5	$P < 0.01$
		30wks (+4)	157.8 ± 6.3	179.2 ± 4.6	$P < 0.05$
	Sb.Pl.Th., lat (μm)	16wks (+4)	113.6 ± 4.1&	168.6 ± 5.5&	$P < 0.01$
		30wks (+4)	112.6 ± 3.0&	150.9 ± 5.1&#	$P < 0.01$
Metaphysis	Trab BV/TV (%)	16wks (+4)	14.0 ± 0.7	15.2 ± 1.6	ns
		30wks (+4)	10.0 ± 0.4#	14.8 ± 0.8	$P < 0.01$
	Tb.Th. (μm)	16wks (+4)	58.3 ± 1.2	63.7 ± 1.3	$P < 0.05$
		30wks (+4)	59.9 ± 0.8	62.9 ± 1.3	ns
	Tb.Sp. (μm)	16wks (+4)	264.9 ± 8.6	329.3 ± 35.2	ns
		30wks (+4)	361.0 ± 7.9#	315.3 ± 25.9	ns
	CD	16wks (+4)	45.5 ± 9.1	59.3 ± 16.7	ns
		30wks (+4)	16.2 ± 4.4#	40.0 ± 5.2	$P < 0.01$
	Ct.Th. (μm)	16wks (+4)	125.8 ± 2.9	157.8 ± 3.2	$P < 0.01$
		30wks (+4)	133.2 ± 1.5	154.1 ± 3.5	$P < 0.01$
Diaphysis	Ct.Th. (μm)	16wks (+4)	192.53 ± 2.4	263.19 ± 5.9	$P < 0.01$
		30wks (+4)	188.36 ± 4.3	261.69 ± 3.2	$P < 0.01$

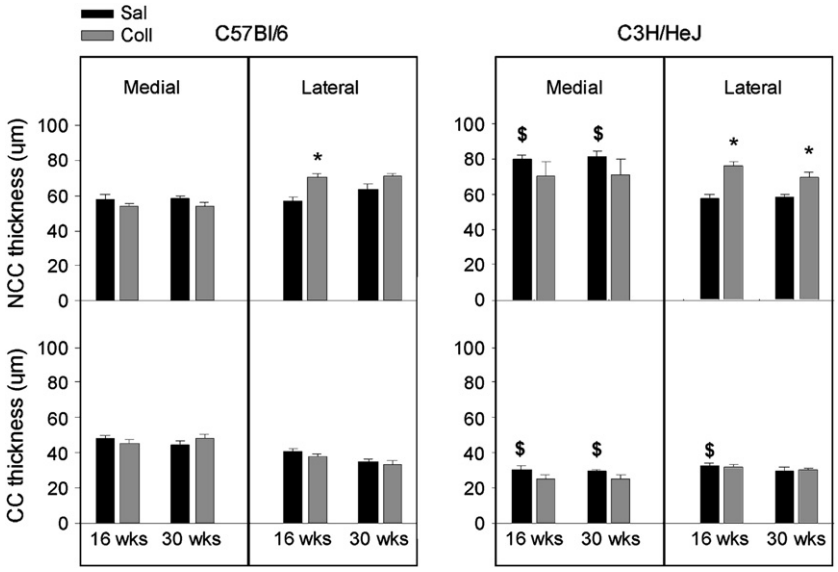

Fig. 2. Thickness of the noncalcified and calcified layers of the articular cartilage at the medial and lateral side in saline-injected and collagenase-injected knee joints. Each bar represents the average (±SEM) of two measurements, one made in anterior region of the knee, and one in the posterior region. Please note the decreased values and increased standard error of the collagenase-injected joints of C3H/HeJ mice at the medial side. In these mice it was sometimes not possible to obtain a thickness value in the postero-medial region due to the severe amount of cartilage damage, in these cases '0' was used as value. Significant differences between saline-injected joints and collagenase-injected joints within strains are indicated by *, between strains of the same age by $. NCC = noncalcified cartilage, CC = calcified cartilage.

joints, whereas the noncalcified layer became thicker at the lateral side, in both strains and at both ages (Fig. 2). At the medial side, no changes were observed.

All C57Bl/6 mice developed spontaneous cartilage damage in the saline-injected joints, with a summed damage score of approx. 10 out of a maximum of 96 at 16 weeks of age (Fig. 3(a), top) that increased to approx. 15 at 30 weeks of age. In contrast, in C3H/HeJ mice spontaneous cartilage damage was virtually absent in all but one mouse at 30 weeks of age. We tested the possibility that the subchondral bone plate thickness of the saline-injected joints was related to the amount of spontaneous cartilage damage, but no relation was found.

In collagenase-injected joints the summed cartilage damage of the whole tibial plateau did not differ significantly between the two strains at either 16 or 30 weeks of age. However, the damage scores of the four separate examined anatomical regions (antero-medial, antero-lateral, postero-medial and postero-lateral) revealed that C57Bl/6 mice had most damage at the lateral side, whereas in C3H/HeJ mice the medial side was the most degenerated (Fig. 3(a), bottom). Besides these differences in spatial arrangement, we also observed a difference in the type of cartilage damage: in C57Bl/6 mice the top layer of the noncalcified cartilage became fibrillated and was loosened in some sections, whereas in C3H/HeJ mice vertical clefts were observed more often. Specifically for C3H/HeJ mice, the postero-medial region showed severe cartilage degeneration with damage scores of 20 or higher out of a maximum of 24. In this region the subchondral bone plate was worn away and the trabecular bone became exposed (Fig. 3(b)). This was not seen in any of the C57Bl/6 mice.

In addition to cartilage damage, osteophytes were observed in all collagenase-injected joints of both mouse strains at both ages. Specifically, at the medial side of the tibia the incidence was 100%. At the lateral side of the tibia the incidence was the same, except for the 30-week-old C57Bl/6 mice in which only five out of eight animals (62.5%) were osteophyte-bearing. In saline-injected joints osteophytes were observed as well, although its sizes were significantly smaller compared to the collagenase-injected joints (data not shown). At 16 weeks of age, these small osteophytes were seen in two out of eight (25%) C57Bl/6 mice at the medial tibia, whereas C3H/HeJ mice of the same age did not have any osteophytes. At the lateral tibia no osteophytes were seen in both strains. At 30 weeks of age, the incidence of small osteophytes became larger with five out of eight (62.5%) C57Bl/6 mice and eight out of eight (100%) C3H/HeJ mice positive at the medial tibia, and one out of eight C57Bl/6 (12.5%) vs two out of eight C3H/HeJ (25%) at the lateral tibia. The mineralized parts of these osteophytes became visible on the micro-CT images as bony outgrowths (see Fig. 1(a), right).

BONE CHANGES IN THE PROXIMAL TIBIA DUE TO INTRA-ARTICULAR COLLAGENASE INJECTION

The subchondral bone plate was significantly thinner in collagenase-injected joints compared to the contralateral saline-injected joints in both strains and at both ages (Fig. 4(a)). The lateral side of the bone plate seemed to be the most affected with a thickness reduction of 12% (16 weeks old) to 18% (30 weeks old) in C57Bl/6 and 20% (16 weeks old) to 24% (30 weeks old) in C3H/HeJ mice. In addition, in 30-week-old C3H/HeJ mice the medial side of the bone plate also became significantly thinner.

Separate analysis at the antero-medial, antero-lateral, postero-medial and postero-lateral regions as done for the assessment of cartilage damage revealed the bone plate thinning to be present throughout the tibial plateau (data not shown). Histological analysis showed TRAP-positive osteoclasts directly underneath the bone plate up to the noncalcified cartilage in collagenase-injected knee joints (Fig. 5). In epiphyses of saline-injected joints osteoclasts were only scarcely observed.

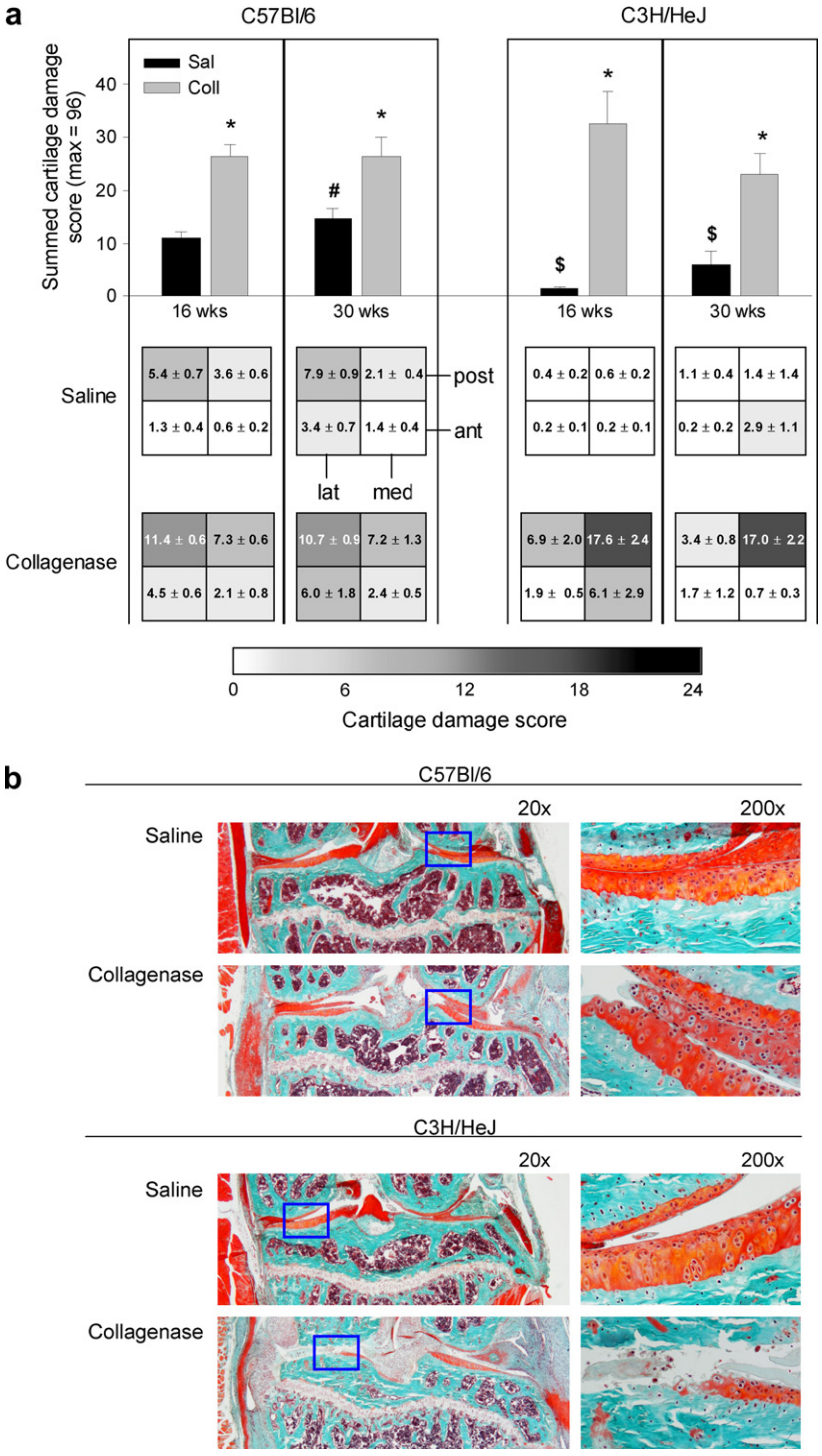

Fig. 3. Cartilage damage in saline-injected knee joints and collagenase-injected knee joints; (a) top: summed cartilage damage score of the antero-lateral, antero-medial, postero-lateral and postero-medial region of the tibial plateau. For each region a maximum score of 24 could be obtained, the maximum obtainable summed score was therefore 96. Significant differences between saline- and collagenase injected joints within strains are indicated by *, between ages within strains by #, between strains of the same age by $; (a) bottom: schematic view of cartilage damage in the four separate regions. For each region the cartilage damage scores (average ± SEM) are depicted in colour-code; (b) histology of the posterior region in knee joints of control and osteoarthritic knee joints. Note the exposure of the subchondral bone at the medial side in collagenase-injected joints of C3H/HeJ mice. The blue boxes indicate a magnification of the lateral (C57Bl/6) and medial (C3H/HeJ) sides, shown on the right.

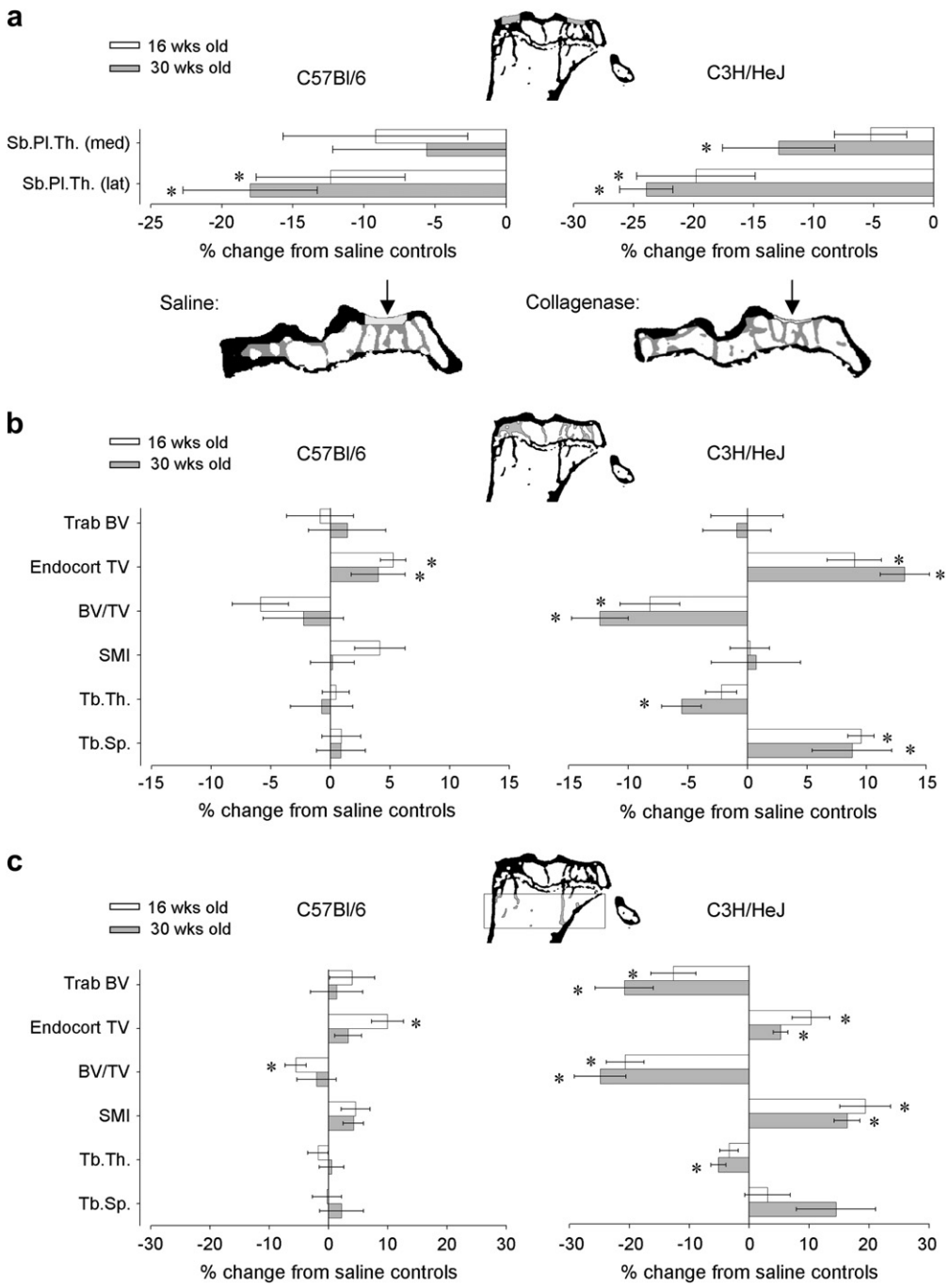

Fig. 4. Bone changes in the proximal tibia expressed as percental change from saline-injected contralateral joints; (a) thickness changes of the medial and lateral subchondral bone plates (Sb.Pl.Th.), with below two examples of thinning of the lateral subchondral bone plate (indicated by arrow) in epiphyses of a saline-injected and collagenase-injected joint from a 30-week-old C57Bl/6 mouse; (b) changes in the epiphyseal trabeculae, the following parameters were measured: trabecular BV (Trab BV), endocortical TV of which the ratio (Trab BV/TV) determines the volumetric amount of bone. Trabecular thickness (Tb.Th.), trabecular spacing (Tb.Sp.), and SMI, indicating the degree of rod-like structure, were also calculated; (c) changes in metaphyseal trabeculae. $^*P < 0.05$.

The epiphyseal trabecular architecture was not altered in C57Bl/6 mice after OA induction, since trabecular BV, thickness, SMI and spacing did not change significantly in either age group (Fig. 4(b), left). However, a small increase of about 5% in endocortical TV was measured compared to the contralateral saline-injected joints, but this did not lead to a significant decrease in Trab BV/TV. An increase in endocortical TV was also observed in collagenase-injected joints of C3H/HeJ mice, lowering the Trab BV/TV ratio to about 10% in both age groups (Fig. 4(b), right). Furthermore, trabeculae in the epiphysis of collagenase-injected C3H/HeJ knee joints were thinner and had increased spacing. Despite these changes in trabecular structure, no significant changes were seen in either connectivity density

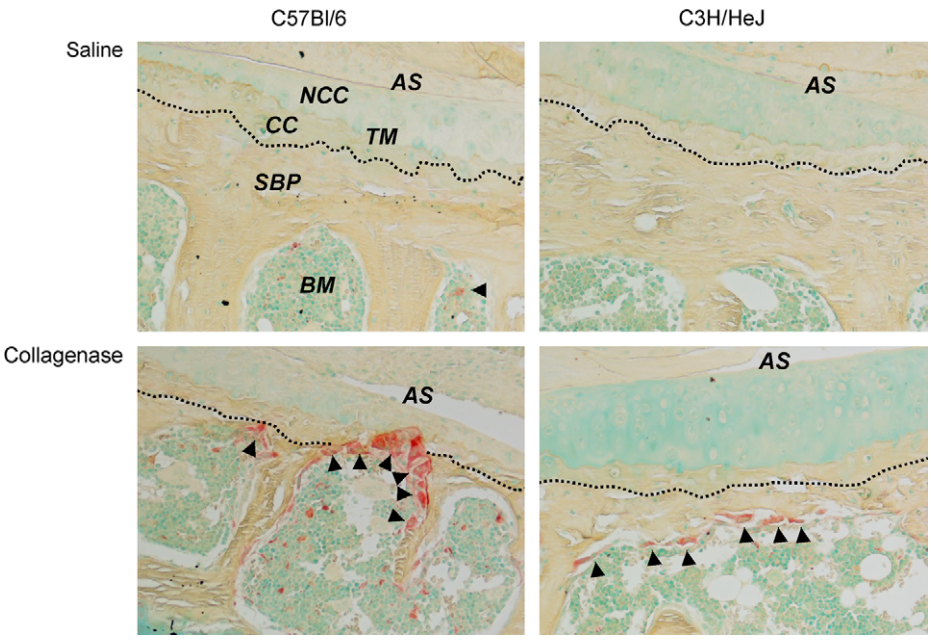

Fig. 5. TRAP staining in histological sections of saline-injected and collagenase-injected knee joints. In saline-injected joints, osteoclasts (arrowheads) were observed occasionally. At some locations in collagenase-injected joints osteoclasts resorbed the subchondral bone plate up to the noncalcified cartilage. The division between the calcified cartilage and the subchondral bone plate is indicated by a dotted line. AS = articular surface, NCC = noncalcified cartilage, CC = calcified cartilage, SBP = subchondral bone plate, TM = tidemark. Original magnification 200×.

or trabecular number (data not shown). Periosteal expansion of the epiphysis other than osteophyte formation was not observed.

In the metaphysis of C57Bl/6 mice the only noticeable change was a small decrease in BV fraction in collagenase-injected joints of the 16-week-old mice caused by an increase in endocortical TV (Endocort TV, Fig. 4(c)). In the metaphysis of C3H/HeJ mice the Endocort TV was also increased in collagenase-injected joints, which together with a reduced Trab BV resulted in a decreased Trab BV/TV of about 20%. In addition, SMI increased, indicating that the metaphyseal trabeculae became more rod-like. In both strains and at both ages the metaphyseal cortex of collagenase-injected joints contained small cavities with TRAP-positive osteoclasts, which were not observed in saline-injected joints. However, the presence of these cavities did not lead to a significant decrease in cortical thickness (data not shown).

BONE CHANGES IN THE DISTAL TIBIA DUE TO INTRA-ARTICULAR COLLAGENASE INJECTION

To verify whether changes in bone also occurred at more remote sites in the joint, e.g., due to differences in limb loading, we measured which changes had occurred in a more distal region of the tibia, the diaphyseal cortex. Although in 16-week-old C57Bl/6 mice the thickness of the diaphyseal cortex in collagenase-injected joints was lower compared to contralateral saline-injected joints (saline-injected: 192 ± 2.4 μm, collagenase-injected: 184 ± 2.1 μm, $P = 0.02$), in all other groups of mice cortical thickness did not differ between saline-injected and collagenase-injected joints. An increase in osteoclastic activity as seen in the subchondral bone plate and the metaphyseal cortex was not observed.

Discussion

This study showed both common findings as well as specific and consistent differences in subchondral bone adaptation and spatial arrangement of cartilage damage between C57Bl/6 mice having an initial thin subchondral bone plate and C3H/HeJ mice having an initial thick subchondral bone plate. In both strains at both ages thinning of the subchondral bone plate was found in collagenase-injected knee joints, but subchondral trabecular changes were only found in C3H/HeJ mice. Both strains developed cartilage damage to a comparable extent, but the spatial arrangement of cartilage damage differed significantly between the two strains: In C57Bl/6 mice the cartilage damage was located mainly at the lateral side of the tibial plateau, both in saline-injected (spontaneous damage) and in collagenase-injected (instability-induced damage) knee joints. In contrast, in C3H/HeJ mice the damage was principally located at the medial side. In these mice spontaneous damage was virtually absent in the saline-injected left control knee joints, so compared to these saline-injected controls the additional damage in the collagenase-injected joints was higher in C3H/HeJ mice.

The reason why we have chosen these two mouse strains was because of their well-described phenotypic difference in bone and subsequent subchondral bone phenotype, a consequence of their different genetic backgrounds[28–32]. Since we know bone to be involved in OA, our initial hypothesis was that a difference in subchondral bone phenotype, and specifically subchondral bone plate thickness, might have an influence on cartilage damage, thereby linking the two. However, when we tested whether the thickness of the subchondral bone plate was related to the amount of cartilage damage, neither in saline-injected nor in collagenase-injected knee joints a relation was found. Besides bone structure, the

mice likely differ in other phenotypical aspects as well such as joint loading and joint alignment. We found a difference in the amount of spontaneous cartilage damage between the two mouse strains and it is tempting to speculate that this might be caused by a difference in joint loading. However, although intuitively logical, there are as yet no literature data available for each of the strains which would substantiate this theory.

Furthermore, differences in joint alignment might explain why there was such a pronounced difference in medial and lateral cartilage damage development. In this view, C57Bl/6 mice place a relative large amount of mechanical load on their lateral tibial plateau, which would increase in the instable collagenase-injected knee joints. This is further supported by the fact that the spatial arrangement of cartilage damage in the saline-injected joints (i.e., spontaneous damage) was the same as in the collagenase-injected joints (i.e., instability-induced damage) within each strain. In C3H/HeJ mice the highest amount of load would be more focal and present on the postero-medial side, explaining the rather drastic amount of cartilage damage seen at the postero-medial region of the tibial plateau in the C3H/HeJ mice.

The composition of the cartilage layer and extracellular matrix might also differ between the two strains. Reports concerning cartilage biology or cartilage mechanical properties in C3H/HeJ mice are scarce and papers comparing these properties between C3H/HeJ and C57Bl/6 are, to our knowledge, non-existing. We demonstrate for the first time a difference in the calcified/noncalcified ratio of the articular cartilage between these two strains. This might influence the stresses in the cartilage resulting from load bearing. Finally, the mechanical properties of joint tendons between the two strains were also found to be different: a recent publication described that joint tendons of C3H/HeJ mice are of inferior quality, although a significant difference in joint laxity between C57Bl/6 and C3H/HeJ mice was not found[33].

In this study we observed that in both strains the subchondral bone plate became thinner in collagenase-injected joints. This was caused by osteoclastic resorption of the subchondral bone plate, at some locations even up to the noncalcified cartilage. Newly formed cavities were observed in the subchondral bone plate, occupied by invading osteoclasts. These cavities might be analogous to the subchondral resorption pits observed in human OA[34]. Whether the mice were 16 or 30 weeks of age at the start of the experiment did not seem to be of influence in either strain, since the direction and magnitude of changes in both bone and cartilage were similar in both age groups. We measured calcified cartilage thickness which, because of its high mineral content[35], cannot be discriminated from bone in micro-CT analysis and found no thickness differences between saline-injected and collagenase-injected joints. Thus, the thickness changes we observed are caused solely by changes in the subchondral bone plate.

There are several explanations for the increased osteoclastic activity in the osteoarthritic joints. One possibility might be a regional acceleratory phenomenon (RAP) due to noxious stimuli such as the stress of surgery or increased amount of inflammation[36]. However, the differences we observed were compared with the saline-injected joints that underwent the same surgical procedure. In addition, although after the collagenase-injection a small inflammatory response is known to occur, this response is only short-lived and is markedly reduced already 3 days after the injection[18]. Therefore, it seems unlikely that RAP plays a role in this process.

Another possibility for increased osteoclastic activity is that the destabilized joint was unloaded, which is known to induce bone resorption[37]. Male C3H/HeJ mice have been shown to lose epiphyseal trabecular bone in response to unloading[38], however, in these models complete unloading is established by hindlimb suspension whereas in our model the mice still had the ability to load their limbs. It is unlikely that a few days of lameness would induce extensive resorptive activity. In addition, the C57Bl/6 strain is known to be more responsive to unloading compared to C3H/HeJ mice[39,40], but in our study the amount of trabecular bone in both the epiphysis and the metaphysis of C57Bl/6 mice was not decreased, and no major changes were found in the thickness of the diaphyseal cortex. We therefore think that unloading does not play an important role and that the bone changes that we have observed are truly part of the disease process.

The fact that we observed subchondral bone plate thinning and increased osteoclastic activity in both strains might be contra-intuitive since subchondral sclerosis is considered as an OA hallmark, but is in fact observed in other animal models of OA as well. Bailey and Mansell identified the formation of subchondral cysts in an early disease stage in guinea pigs[41], which might indicate initial weakening of the subchondral bone. They stated that subchondral bone thickening might be a compensatory response observed later on in the disease process. This theory was confirmed in a rat model in which anterior cruciate ligament transection (ACLT) was performed[42] and in a canine model using the same approach[43,44]. Interestingly, these studies also found sclerosis of the subchondral bone to occur eventually. Recovery of initial loss of subchondral bone was seen in a post-traumatic OA model in rabbits as well[45], with initial bone loss followed by bone accrual and subsequent sclerosis later on. Lastly, a feline study also showed subchondral plate thinning[46] at 16 weeks following ACLT.

These beforementioned studies suggest that the OA disease process in our study is likely to be in an early phase, whereas in human studies the disease has already progressed further. Other lines of evidence from our study further confirm this hypothesis: first, even though the instability-induced cartilage damage was clearly present in both strains and C3H/HeJ mice had severe amounts of cartilage damage locally, the summed cartilage damage was still quite low, approximately 25 whereas a maximum score of 96 could be obtained. Second, the process of cartilage wear and tear was still in an early phase, as indicated by the swelling of the noncalcified cartilage layer in collagenase-injected joints (see Fig. 2), a known feature of early OA[47,48]. Finally, the osteophytes that were formed in the collagenase-injected joints were not yet fully mineralized, indicating an immature stage of osteophyte development.

In summary, we evaluated changes in bone and cartilage 4 weeks after OA induction in two strains of mice having a different subchondral bone phenotype. The subchondral bone plate was found to become thinner in both strains, but the spatial distribution of cartilage damage after OA induction was found to differ significantly. The observed thinning was not linked to the location and severity of cartilage damage in either strain, but seemed to be a diffuse event taking place across the whole tibial plateau.

Acknowledgments

We acknowledge Jan-Floris de Graaf for assisting in the analysis of the bone morphometric data, Nicole Kops for

helping with histology and the personnel of the Experimental Animal Facility of the Erasmus MC for taking care of the animals during the experiment.

References

1. Odding E, Valkenburg HA, Stam HJ, Hofman A. Determinants of locomotor disability in people aged 55 years and over: the Rotterdam Study. Eur J Epidemiol 2001;17:1033–41.
2. Radin EL, Rose RM. Role of subchondral bone in the initiation and progression of cartilage damage. Clin Orthop 1986;34–40.
3. Grynpas MD, Alpert B, Katz I, Lieberman I, Pritzker KPH. Subchondral bone in osteoarthritis. Calcif Tissue Int 1991;49:20–6.
4. Day JS, Ding M, van der Linden JC, Hvid I, Sumner DR, Weinans H. A decreased subchondral trabecular bone tissue elastic modulus is associated with pre-arthritic cartilage damage. J Orthop Res 2001; 19:914–8.
5. Li B, Marshall D, Roe M, Aspden RM. The electron microscope appearance of the subchondral bone plate in the human femoral head in osteoarthritis and osteoporosis. J Anat 1999;195(Pt 1):101–10.
6. Bobinac D, Spanjol J, Zoricic S, Maric I. Changes in articular cartilage and subchondral bone histomorphometry in osteoarthritic knee joints in humans. Bone 2003;32:284–90.
7. Ding M, Odgaard A, Hvid I. Changes in the three-dimensional microstructure of human tibial cancellous bone in early osteoarthritis. J Bone Joint Surg Br 2003;85:906–12.
8. Carlson CS, Loeser RF, Purser CB, Gardin JF, Jerome CP. Osteoarthritis in cynomolgus macaques. III: effects of age, gender, and subchondral bone thickness on the severity of disease. J Bone Miner Res 1996;11:1209–17.
9. Layton MW, Goldstein SA, Goulet RW, Feldkamp LA, Kubinski DJ, Bole GG. Examination of subchondral bone architecture in experimental osteoarthritis by microscopic computed axial tomography. Arthritis Rheum 1988;31:1400–5.
10. Anderson-Mackenzie JM, Quasnichka HL, Starr RL, Lewis EJ, Billingham ME, Bailey AJ. Fundamental subchondral bone changes in spontaneous knee osteoarthritis. Int J Biochem Cell Biol 2005;37: 224–36.
11. Fahlgren A, Messner K, Aspenberg P. Meniscectomy leads to an early increase in subchondral bone plate thickness in the rabbit knee. Acta Orthop Scand 2003;74:437–41.
12. Wachsmuth L, Engelke K. High-resolution imaging of osteoarthritis using microcomputed tomography. Methods Mol Med 2004;101:231–48.
13. Naitou K, Kushida K, Takahashi M, Ohishi T, Inoue T. Bone mineral density and bone turnover in patients with knee osteoarthritis compared with generalized osteoarthritis. Calcif Tissue Int 2000;66:325–9.
14. Hochberg MC, Lethbridge-Cejku M, Tobin JD. Bone mineral density and osteoarthritis: data from the Baltimore Longitudinal Study of Aging. Osteoarthritis Cartilage 2004;12(Suppl A):S45–8.
15. Hart DJ, Cronin C, Daniels M, Worthy T, Doyle DV, Spector TD. The relationship of bone density and fracture to incident and progressive radiographic osteoarthritis of the knee: the Chingford Study. Arthritis Rheum 2002;46:92–9.
16. Burger H, van Daele PL, Odding E, Valkenburg HA, Hofman A, Grobbee DE, *et al.* Association of radiographically evident osteoarthritis with higher bone mineral density and increased bone loss with age. The Rotterdam Study. Arthritis Rheum 1996;39:81–6.
17. Bergink AP, Uitterlinden AG, van Leeuwen JP, Hofman A, Verhaar JA, Pols HA. Bone mineral density and vertebral fracture history are associated with incident and progressive radiographic knee osteoarthritis in elderly men and women: the Rotterdam Study. Bone 2005;37: 446–56.
18. Van der Kraan PM, Vitters EL, Vanbeuningen HM, Vandeputte LBA, Van den Berg WB. Degenerative knee-joint lesions in mice after a single intraarticular collagenase injection – a new model of osteoarthritis. J Exp Pathol 1990;71:19–31.
19. Van Osch GJ, Van der Kraan PM, Vitters EL, Blankevoort L, Van den Berg WB. Induction of osteoarthritis by intra-articular injection of collagenase in mice Strain and sex related differences. Osteoarthritis Cartilage 1993;1:171–7.
20. Van Osch GJ, Blankevoort L, Van der Kraan PM, Janssen B, Hekman E, Huiskes R, *et al.* Laxity characteristics of normal and pathological murine knee joints *in vitro*. J Orthop Res 1995;13:783–91.
21. Van Osch GJ, Van der Kraan PM, Blankevoort L, Huiskes R, Van den Berg WB. Relation of ligament damage with site specific cartilage loss and osteophyte formation in collagenase induced osteoarthritis in mice. J Rheumatol 1996;23:1227–32.
22. Van Osch GJ, Van der Kraan PM, Van den Berg WB. Site-specific cartilage changes in murine degenerative knee joint disease induced by iodoacetate and collagenase. J Orthop Res 1994;12:168–75.
23. Waarsing J, Day J, Weinans H. An improved segmentation method for *in-vivo* micro-CT imaging. J Bone Miner Res 2004.
24. Odgaard A, Gundersen HJ. Quantification of connectivity in cancellous bone, with special emphasis on 3-D reconstructions. Bone 1993;14: 173–82.
25. Hildebrand T, Ruegsegger P. Quantification of bone microarchitecture with the structure model index. Comput Methods Biomech Biomed Engin 1997;1:15–23.
26. Pritzker KP, Gay S, Jimenez SA, Ostergaard K, Pelletier JP, Revell PA, *et al.* Osteoarthritis cartilage histopathology: grading and staging. Osteoarthritis Cartilage 2006;14:13–29.
27. Scheven BA, Kawilarang-De Haas EW, Wassenaar AM, Nijweide PJ. Differentiation kinetics of osteoclasts in the periosteum of embryonic bones *in vivo* and *in vitro*. Anat Rec 1986;214:418–23.
28. Chen C, Kalu DN. Strain differences in bone density and calcium metabolism between C3H/HeJ and C57BL/6J mice. Bone 1999;25:413–20.
29. Richman C, Kutilek S, Miyakoshi N, Srivastava AK, Beamer WG, Donahue LR, *et al.* Postnatal and pubertal skeletal changes contribute predominantly to the differences in peak bone density between C3H/HeJ and C57BL/6J mice. J Bone Miner Res 2001;16:386–97.
30. Sheng MH, Lau KH, Beamer WG, Baylink DJ, Wergedal JE. *In vivo* and *in vitro* evidence that the high osteoblastic activity in C3H/HeJ mice compared to C57BL/6J mice is intrinsic to bone cells. Bone 2004; 35:711–9.
31. Koller DL, Schriefer J, Sun Q, Shultz KL, Donahue LR, Rosen CJ, *et al.* Genetic effects for femoral biomechanics, structure, and density in C57BL/6J and C3H/HeJ inbred mouse strains. J Bone Miner Res 2003;18:1758–65.
32. Akhter MP, Iwaniec UT, Covey MA, Cullen DM, Kimmel DB, Recker RR. Genetic variations in bone density, histomorphometry, and strength in mice. Calcif Tissue Int 2000;67:337–44.
33. Wang VM, Banack TM, Tsai CW, Flatow EL, Jepsen KJ. Variability in tendon and knee joint biomechanics among inbred mouse strains. J Orthop Res 2006;24:1200–7.
34. Shibakawa A, Yudoh K, Masuko-Hongo K, Kato T, Nishioka K, Nakamura H. The role of subchondral bone resorption pits in osteoarthritis: MMP production by cells derived from bone marrow. Osteoarthritis Cartilage 2005;13:679–87.
35. Burr DB. Anatomy and physiology of the mineralized tissues: role in the pathogenesis of osteoarthrosis. Osteoarthritis Cartilage 2004; 12(Suppl A):S20–30.
36. Frost HM. The regional acceleratory phenomenon: a review. Henry Ford Hosp Med J 1983;31:3–9.
37. Bikle DD, Halloran BP. The response of bone to unloading. J Bone Miner Metab 1999;17:233–44.
38. Squire M, Donahue LR, Rubin C, Judex S. Genetic variations that regulate bone morphology in the male mouse skeleton do not define its susceptibility to mechanical unloading. Bone 2004;35:1353–60.
39. Judex S, Garman R, Squire M, Busa B, Donahue LR, Rubin C. Genetically linked site-specificity of disuse osteoporosis. J Bone Miner Res 2004;19:607–13.
40. Amblard D, Lafage-Proust MH, Laib A, Thomas T, Ruegsegger P, Alexandre C, *et al.* Tail suspension induces bone loss in skeletally mature mice in the C57BL/6J strain but not in the C3H/HeJ strain. J Bone Miner Res 2003;18:561–9.
41. Bailey AJ, Mansell JP. Do subchondral bone changes exacerbate or precede articular cartilage destruction in osteoarthritis of the elderly? Gerontology 1997;43:296–304.
42. Hayami T, Pickarski M, Zhuo Y, Wesolowski GA, Rodan GA, Duong le T. Characterization of articular cartilage and subchondral bone changes in the rat anterior cruciate ligament transection and meniscectomized models of osteoarthritis. Bone 2006;38:234–43.
43. Dedrick DK, Goldstein SA, Brandt KD, O'Connor BL, Goulet RW, Albrecht M. A longitudinal study of subchondral plate and trabecular bone in cruciate-deficient dogs with osteoarthritis followed up for 54 months. Arthritis Rheum 1993;36:1460–7.
44. Dedrick DK, Goulet RW, O'Connor BL, Brandt KD. Preliminary report: increased porosity of the subchondral plate in an accelerated canine model of osteoarthritis. Osteoarthritis Cartilage 1997;5:71–4.
45. Batiste DL, Kirkley A, Laverty S, Thain LM, Spouge AR, Holdsworth DW. *Ex vivo* characterization of articular cartilage and bone lesions in a rabbit ACL transection model of osteoarthritis using MRI and micro-CT. Osteoarthritis Cartilage 2004;12:986–96.
46. Boyd SK, Muller R, Leonard T, Herzog W. Long-term periarticular bone adaptation in a feline knee injury model for post-traumatic experimental osteoarthritis. Osteoarthritis Cartilage 2005;13:235–42.
47. Calvo E, Palacios I, Delgado E, Ruiz-Cabello J, Hernandez P, Sanchez-Pernaute O, *et al.* High-resolution MRI detects cartilage swelling at the early stages of experimental osteoarthritis. Osteoarthritis Cartilage 2001;9:463–72.
48. Bush PG, Hall AC. The volume and morphology of chondrocytes within non-degenerate and degenerate human articular cartilage. Osteoarthritis Cartilage 2003;11:242–51.